

# Simulating Turbulent Flow over Thin Element and Flat Valley V-Shaped Riblets

A. Pollard\*

*Queen's University at Kingston, Kingston, Ontario K7L 3N6, Canada*

A. M. Savill†

*Cambridge University, Cambridge CB2 1PZ, England, United Kingdom*  
and

S. Tullis‡ and X. Wang§

*Queen's University at Kingston, Kingston, Ontario K7L 3N6, Canada*

The time-dependent flow over riblets of various shapes is calculated using a control volume finite element simulation technique and assuming a model of the near-wall viscous flow region of a turbulent boundary layer. The cross-sectional shapes considered include thin element blade riblets and saw-toothed riblets (but with flat valleys), which are similar to the more common continuous V-shaped riblets. Turbulence statistics derived from the calculations include skewness and flatness factors. It is concluded that to achieve maximum drag reduction, riblets not only need to ensure a thicker than usual viscous laminar-like flow in their grooves, but also the transient momentum exchange must be minimized between this inner region and the larger-scale outer motions associated with quasistreamwise vortices.

## I. Introduction

IT is now well established that streamwise aligned microgrooves on the surface of a body decrease skin-friction drag by about 8–10%.<sup>1</sup> However, the physical reasons why these grooves achieve this level of friction reduction are still not fully understood. Thus, although a reasonable number of riblet geometries have been tested experimentally (for two-dimensional examples, see Walsh<sup>2</sup>; for three-dimensional examples, see Enyutin et al.<sup>3</sup> and Bechert<sup>4</sup>; several simple geometries have been studied computationally by Tullis and Pollard,<sup>5–7</sup> Chu and Karniadakis,<sup>8</sup> Chu et al.,<sup>9</sup> and Choi et al.<sup>10</sup>), it is not yet clear what limits the skin-friction reduction and how exactly each geometry interacts with the very near-wall structures of the turbulent boundary layer. Although several detailed experimental investigations have been performed, for example, Refs. 11–16, it has been so far impossible to unambiguously determine the influence of the riblets on the sequence of the motions comprising the regenerative turbulent burst cycle, in a manner described by Refs. 17–19, for the flat wall, zero-pressure-gradient turbulent boundary layer.

In this paper, the near-wall simulation approach of Tullis and Pollard<sup>5</sup> is applied to riblets of three different cross-sectional shapes. This time-dependent computational methodology provides a method of gaining insight into the interaction of the laminar-like regime<sup>20</sup> and the incursion of the outer region ( $y^+ \geq 20$ , say) turbulent eddies into the grooves. This interaction is traced using higher-order statistics that reveal that the skewness in the longitudinal velocity component is considerably affected by the shape and spacing of the riblet geometry.

## II. Near-Wall Turbulence and Riblets

Documentation of the basic features of low-Reynolds-number turbulent boundary layers is adequately described in Refs. 13 and 21–23. Although there is Reynolds number dependence on the scales of the structures, it is generally agreed that the dominant feature in

the near-wall region outside the buffer layer are quasistreamwise vortices (QSWVs). These vortices have a typical spanwise spacing of  $\lambda^+ \approx 100$ , where the usual nondimensional form applies, and have a length-to-diameter ratio of about 10 and a mean diameter of  $d^+ \approx 30$ . Robinson<sup>23</sup> presents a histogram of diameters, vortex Reynolds numbers, etc. These QSWVs are, of course, neither fixed in space nor continuously identifiable: they are convected by and at various angles to the mean flow and they evolve through a birth/death cycle, each giving rise to new QSWVs. This is a simplistic view, of course, and the reader is referred to the preceding references for more details.

The picture that is beginning to emerge from the work performed so far on riblets is that a large region of the flow inside the grooves is essentially laminar<sup>20,24</sup> and that this region tends to isolate the wall from shearing action of the QSWV.<sup>5–7</sup> The wider the spacing between the riblets ( $s^+$ ), the greater the incursion of these QSWVs, with a concomitant diminution in the skin-friction drag reduction benefits from the maximum reduction of  $\approx 8\%$  at  $s^+ \approx 12$  to perhaps 30, depending on the riblet geometry; see, for example, Ref. 25. When the QSWVs enter directly within the riblets, the turbulence level suddenly increases there,<sup>26</sup> and the drag switches from a being beneficial (reduction) to a liability (increase). Note that Robinson found that the histogram of QSWVs revealed that 70% of them had diameters  $d^+ \leq 40$ , with 25% having  $d^+ \leq 20$ . Thus, although Choi et al.<sup>10</sup> argue that the mean diameters of the QSWVs ( $d^+ \approx 30$ ) are such that most will stay above the grooves ( $s^+ = 20$ ), thereby not exposing much of the riblet tips to the sweeping motion of the QSWVs, it is not clear why a riblet spacing of  $s^+ \approx 12$  actually gives the maximum diminution in skin friction.

As noted earlier, there have been various studies of riblets of different cross-sectional shape, and it is clear, particularly from the work of Walsh,<sup>2</sup> that for the maximum benefit these must have sharp peaks, but provided this criterion is met, similar levels of reduction can be achieved with a variety of actual profile shapes. Thus V-groove-type riblets give similar skin-friction reductions to V grooves with a flat valley and U and L groove riblets (see, for example, Coustols and Savill<sup>1</sup>). Thin element riblets, however, may offer some advantages in terms of skin-friction reduction if they include smaller interriblet elements as proposed by Savill.<sup>27</sup> This proposition has recently been confirmed experimentally<sup>25</sup> and computationally.<sup>6</sup> It appears that the combination of two large riblets that bracket a smaller riblet, placed midway between the two larger riblets, will produce the same effect of a larger riblet, but

Received June 16, 1995; revision received April 25, 1996; accepted for publication April 25, 1996; also published in *AIAA Journal on Disc*, Volume 1, Number 4. Copyright © 1996 by the authors. Published by the American Institute of Aeronautics and Astronautics, Inc., with permission.

\*Professor, Department of Mechanical Engineering.

†Senior Research Fellow, Engineering Department.

‡Graduate Student, Department of Mechanical Engineering.

§Researcher, Department of Mechanical Engineering.

without the added deleterious effects of increased whetted area and concomitant shear stress.

Direct numerical simulations (DNSs) of flow over plain walls and walls populated by riblets by Chu and Karniadakis<sup>8</sup> and Choi et al.<sup>10</sup> have produced some conflicting results: the former find that there are significant numbers of negative streamwise velocity events inside the riblet valleys, whereas the latter do not. The near-wall turbulence statistics of the former do not collapse to a single curve on the wall unpopulated by riblets, whereas the latter do. In addition, the probability density distributions for the velocity components ( $y^+ \leq 40$ ) in the former case are distinctly different in both magnitude and in some places in sign to the experimental data of Choi.<sup>13</sup> DNS results were integrated over 600 and 4000 viscous time units in Refs. 8 and 10, respectively, which suggests that the latter results are probably more reliable.

In this paper, the near-wall viscous region is modeled by solving a restricted form of the Navier–Stokes equations in time, where the restriction is the imposition of a modeled external boundary condition that mimicks the action of the QSWV and assumes that the flow is periodic both in time and in the lateral or spanwise space direction. The Navier–Stokes equations are solved between the nonslip surface and modeled external boundary using a triangular element control volume method. This model is applied to a flat wall turbulent boundary layer ( $y^+ \leq \sim 40$ ) and to walls populated by riblets. The time-averaged statistics are computed and compared against experimental data and the effects of riblets on the QSWV (and vice versa) estimated.

### III. Modeling Approach and Numerical Solution

The Navier–Stokes equations, in their spatially parabolic form in two dimensions, are solved using a control volume finite element method. The boundary conditions specified over the domain include zero slip at any fluid–wall interface, periodicity in directions parallel to the wall, and the imposition of a two-scale, outer region driven eddy model along a line located about (dependent upon the riblet shape)  $y^+ \simeq 40$ . The spanwise extent of the domain is on the order of 100–200 wall units.<sup>28,29</sup>

The main modeling assumption of the method is in the specification of the velocities along the upper,  $y_0$ , edge of the domain. These specifications can vary slightly; however, the fluctuating velocity components specified at the upper boundary are periodic in time and spanwise location and are representative of quasiperiodic streamwise vortices. Consequently, the specifications are intended to not exactly model the flow in this region but to provide a model of the eddy structure in the viscous wall region:

$$U_e = \bar{U}_e + \hat{u}_1 \cos[(2\pi/T_1)t + \phi_{u1}] \cos(2\pi/\lambda_1)z \\ + \hat{u}_2 \cos[(2\pi/T_2)t + \phi_{u2}] \cos(2\pi/\lambda_2)z \quad (1)$$

$$v_e = \hat{v}_1 \cos[(2\pi/T_1)t + \phi_{v1}] \cos(2\pi/\lambda_1)z \\ + \hat{v}_2 \cos[(2\pi/T_2)t + \phi_{v2}] \cos(2\pi/\lambda_2)z \quad (2)$$

$$w_e = \hat{w}_1 \cos[(2\pi/T_1)t + \phi_{w1}] \sin(2\pi/\lambda_1)z \\ + \hat{w}_2 \cos[(2\pi/T_2)t + \phi_{w2}] \sin(2\pi/\lambda_2)z \quad (3)$$

where  $U_e$ ,  $v_e$ , and  $w_e$  are the specified upper edge velocities,  $\lambda_1$  and  $\lambda_2$  are the spanwise periods, and  $T_1$  and  $T_2$  are the time periods for each of the two eddy scales. Each of the time periodicities (fluctuations) has a phase angle  $\phi$  relative to some reference cycle. There are also the amplitudes ( $\hat{u}_1$ ,  $\hat{u}_2$ ,  $\hat{v}_1$ ,  $\hat{v}_2$ ,  $\hat{w}_1$ , and  $\hat{w}_2$ ) for each velocity component for each of the two scales. The model of Chapman and Kuhn<sup>28</sup> does not use all terms in Eq. (2); see Tullis.<sup>30</sup>

Other than the imposition of the domain upper boundary condition, there are no assumptions made: the Navier–Stokes equations are solved completely, subject to the constraints of two-dimensionality, spanwise periodicity, and numerical approximation. The treatment of the wall surface uses the protrusion height concept<sup>24</sup> to define an effective origin for the riblet surface.

The numerical method used to solve the preceding equation set and its boundary conditions is an equal order control volume finite element method.<sup>30,31</sup> This approach uses triangular elements that

permit the riblet geometry to be exactly fitted, within the limit of small straight-line segments.

The size of the computational domain was specified as  $0 \leq y \leq (40 + h - h_p)$  in the wall normal direction and  $0 \leq z \leq 100$  in the spanwise direction. Various computational grids were used; typically  $32 \times 81$  control volumes in the wall normal and spanwise directions with nonuniform grouping near the riblet peaks. The typical (nondimensional) spacing between the velocity flux locations and the control volume surface is typically  $\Delta y \approx \Delta z = 0.7$ ; however, near the wall, the values can be less, depending on the riblet configuration considered. Various grids have been tried,<sup>30</sup> and the value quoted gives grid independent results; note that, in finite volume DNS, grid spacings of about the same magnitude are employed.<sup>10</sup>

Time steps of  $1 \leq \Delta t \leq 4$  were attempted. From a comparison of solutions run for a total time span of approximately 100t (recall this is in wall units), little difference was apparent between the solutions obtained using time step sizes of  $\Delta t = 1, 2$ , and 4. Calculated pressures and downstream momenta at two locations in the middle of the computational domain were compared for the  $\Delta t = 1$  and 2 cases with the maximum differences being approximately 1–2%. All results are thus presented for  $\Delta t = 2$ .

At  $t = 0$ , the fluctuating velocity components were set to zero throughout the computational domain. The solution to the resulting Laplace equation for the downstream momentum  $U$  is just Couette flow with the upper velocity being the specified mean value along the upper boundary. The effect of this initial solution on any statistics was not apparent after two of the larger-scale eddy periods ( $T_2 = 286$ ). The solution in the computational domain also becomes periodic in time matching the full ( $T_2$ ) periodicity of the upper boundary conditions. Consequently all statistics were taken for a time interval of one larger eddy scale period starting after at least three of these time periods.

### IV. Presentation and Discussion of Results

Attention is first placed on the ability of the technique to recreate the main time-averaged features of a zero-pressure-gradient turbulent boundary layer. These comparisons are provided in Figs. 1 and 2, where the normalized Reynolds normal and shear stresses are plotted against data from Gupta and Kaplan,<sup>32</sup> Ueda and Hinze,<sup>33</sup> and Baron and Quadrio,<sup>34</sup> as well as the DNS calculations from Choi et al.<sup>10</sup> The present calculations are in quite acceptable accord with previous work, except perhaps for  $v'$  and  $w'$ ; however, although the magnitudes of these latter two quantities differ from those data sets considered, the trends are certainly well predicted. Note that measurement of the wall normal velocity is difficult. A more stringent test of the present near-wall model is the ability to recreate the skewness  $S_u$  and flatness  $F_u$  factors of the longitudinal velocity. Figures 3 and 4 provide a comparison between the calculations and the experimental data of Ueda and Hinze<sup>33</sup> and Baron and Quadrio<sup>34</sup> and the DNS calculations of Choi et al.<sup>10</sup> Skewness,

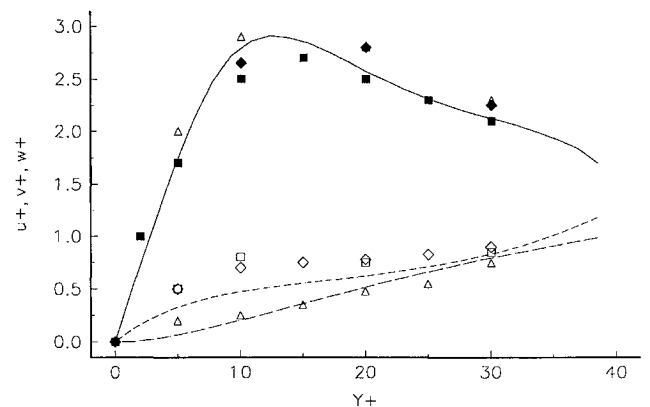
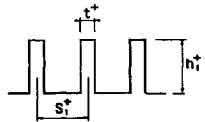
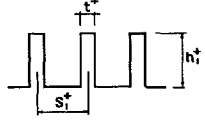
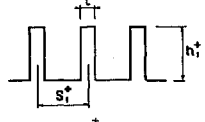
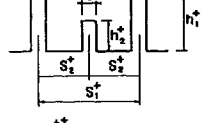
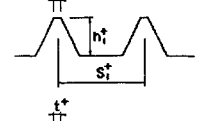
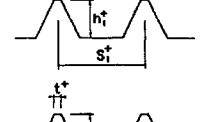
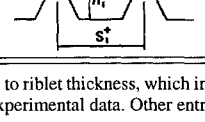
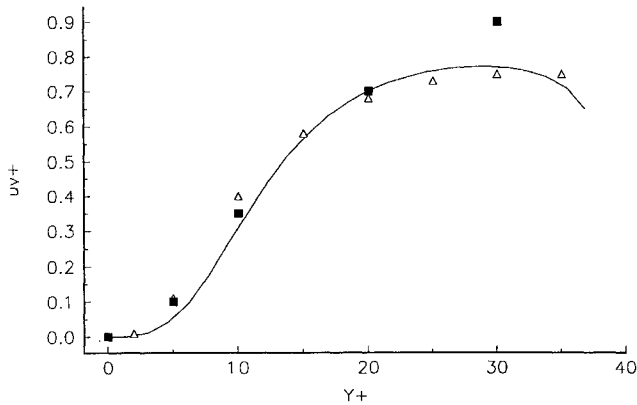


Fig. 1 Comparison of calculations using near-wall viscous model against flat wall turbulent boundary-layer data: normalized fluctuating velocities vs distance from the wall: —,  $u$ -NWVM;  $\Delta$ ,  $u$ -Gupta and Kaplan<sup>32</sup>;  $\blacksquare$ ,  $u$ -Choi et al.<sup>10</sup>;  $\blacklozenge$ ,  $u$ -Ueda and Hinze<sup>33</sup> (average); —,  $v$ -NWVM;  $\square$ ,  $v$ -Gupta and Kaplan<sup>32</sup>;  $\diamond$ ,  $v$ -Choi et al.<sup>10</sup>; - - -,  $w$ -NWVM; and  $\circ$ ,  $w$ -Choi et al.<sup>10</sup>

**Table 1** Cross-sectional shapes of riblets, their nondimensional sizes ( $h^+$  and  $t^+$ ) and spacing ( $s^+$ ), and their protrusion heights ( $h_p^+$ )<sup>a</sup>

No.	Riblet shape	$h_1^+$	$h_2^+$	$s_1^+$	$s_2^+$	$t^+$	$h_p^+$	Ref.
1		16.7	—	33.3	—	2.4	6.0	37, 40
2		10.0	—	12.5	—	1.0	2.3	40
3		15.0	—	20.0	—	0	4.41	—
4		16.7	8.3	33.3	16.7	2.4	2.5(?)	40
5		20.9	—	33.3	—	1.0	5.83	12
6		15.0	—	20.0	—	0	3.99	—
7		9.0	—	14.3	—	0	2.79	12

<sup>a</sup> $t^+$  refers to riblet thickness, which in the flat valley V-groove case is the width of the land on top surface. References refer to experimental data. Other entries indicate that only computations are available.



**Fig. 2** Comparison of calculations using near-wall viscous model against flat wall turbulent boundary-layer data: normalized Reynolds shear stress vs distance from the wall: —,  $uv$ -NWVM;  $\Delta$ ,  $uv$ -Choi et al.<sup>10</sup>; and  $\blacksquare$ ,  $uv$ -Gupta and Kaplan.<sup>32</sup>

the third moment of velocity or the first measure of asymmetry in a probability density distribution, can be related to structural events by noting that a positive value implies that there are many more small positive than the equivalent negative events, outside the standard deviation. Flatness, the fourth moment of velocity, is a measure of the peakedness of a distribution relative to a normal one (flatness factor = 3) and, hence, is indicative of the relative importance of the small events in the tails of the distribution (large deviation from the mean).

From the figures provided, the skewness factor is seen to be in acceptable agreement with the data; however, the flatness factor is at odds with the available data as a result of the boundary condition

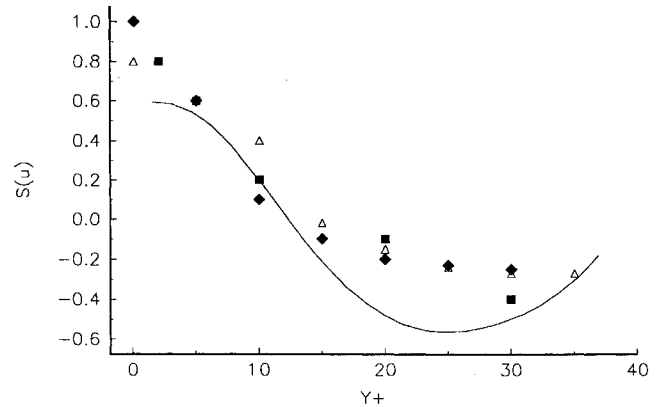


**Fig. 3** Comparison of calculations using near-wall viscous model against flat wall turbulent boundary-layer data: skewness in streamwise fluctuating velocity vs distance from the wall: —,  $S(u)$  NWVM;  $\Delta$ ,  $S(u)$  Choi et al.<sup>10</sup>;  $\blacksquare$ ,  $S(u)$  Ueda and Hinze<sup>33</sup>; and  $\blacklozenge$ ,  $S(u)$  Baron and Quadrio.<sup>34</sup>

specified at  $y = 40$ . This is simply harmonic and cannot faithfully represent the intermittent nature of the wallward sweep portion of the QSWV. Even so, the streaky-like structure in the near wall is reasonably well captured by the present calculations. The time-dependent meandering of the low-speed streaks ( $\approx 20$ – $30$  wall units) can be discerned,<sup>30</sup> and the duration of the streak is about 1500 wall units, in good agreement with experiments<sup>21,22</sup> and the DNS results of Ref. 23.

The streak-like structure of the low-speed flow is in contrast to the much wider and shorter lived intrusions of high-speed fluid towards the wall. These intrusions are generally associated with the wallward

flow between two counter-rotating vortices and consequently appear to exist only while both vortices are present. The relatively large spanwise size of these features ( $\sim 50$  wall units) can be explained by their association with the pair of vortices and the convection of the high downstream momentum fluid, not just between but also underneath them. The wallward flow between the vortices leads to the creation of a high-pressure region at the wall preceding the impact or "splat" of the high downstream momentum fluid with the wall. The splat is either similar or equivalent to a Q4 event if quadrant analysis is invoked.<sup>35</sup> This explanation of the contrast between the low-speed streaks and high-speed splats is based only on the behavior of the cross-stream vortex flows because the downstream momentum is

treated here as a scalar quantity convected by and diffusing through the cross-stream flow.

Calculations have been performed for the riblet shapes indicated in Table 1. The boundary conditions are the same as for the plain wall case, except that the boundary condition along the upper surface of the computational domain is shifted upwards ( $y = 40 + h - h_p$ ). That this upper condition should remain as for the flat wall case is confirmed by experimental evidence, which demonstrates that flat wall and riblet wall results are indistinguishable above  $y^+ \approx 40$ .<sup>15,36,37</sup> The ability of the model and the approach taken have been previously reported,<sup>5-7</sup> against the hot wire data,<sup>15,36</sup> where it was demonstrated that the streamwise velocities (mean and rms) were found in good accord with the data.

To assist in placing into perspective the present calculations, the model predictions are compared against those particle tracking velocimetry (PTV) data of Suzuki and Kasagi.<sup>12,38</sup> These authors have obtained data for two riblet sizes,  $s = 31, h = 19$  and  $s = 15, h = 9.1$  (nondimensionalized). The modeled riblets do not exactly correspond to those used in the experiments; here  $s = 33.3, h = 20.9$ , and  $t = 1$  and  $s = 14.3, h = 9.0$ , and  $t = 0$  as summarized in Table 1. The slight difference is a result of grid generation limitations. The PTV data are ensemble averaged using between 120–240 realizations at random points in the flow. These data were then summed within bins, 0.2 mm wide ( $\delta y \sim 1.75$ , which is a little better spatially averaged than data obtained using hot wires<sup>39</sup>) over a uniformly distributed distance between the peak and the valley of the riblet. It is claimed that at each location over 6000 realizations give sufficient data from which time-averaged statistics can be generated. However, it is unclear whether indeed the statistics are unbiased.

In Figs. 5 and 6 the axial mean and rms velocities are compared with the data. The experimental maximum value of the rms axial velocity is approximately 2.25 while equal to 2.75 from both hot wire data obtained over riblets of about the same spacing and the calculations.

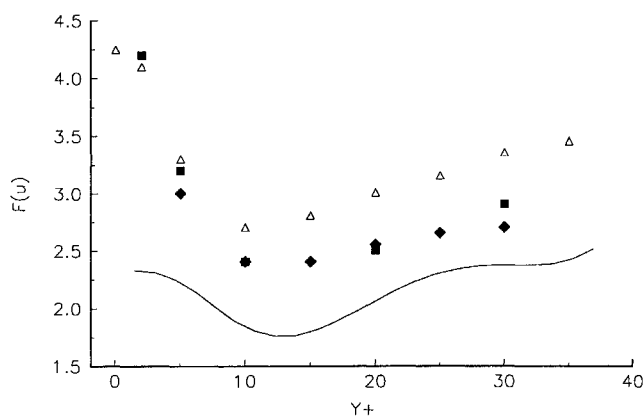
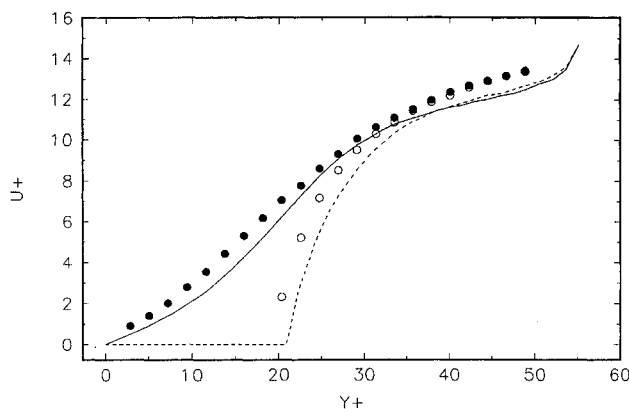
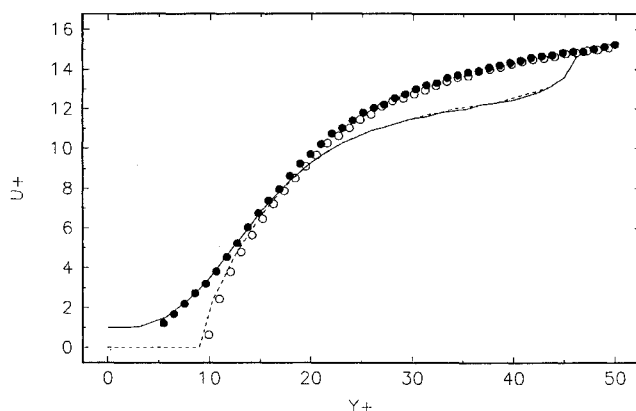


Fig. 4 Comparison of calculations using near-wall viscous model against flat wall turbulent boundary-layer data: flatness factor for streamwise fluctuating velocity vs distance from the wall: —,  $F(u)$  NWVM;  $\Delta$ ,  $F(u)$  Choi et al.<sup>10</sup>;  $\blacksquare$ ,  $F(u)$  Ueda and Hinze<sup>33</sup>; and  $\blacklozenge$ ,  $F(u)$  Baron and Quadrio.<sup>34</sup>

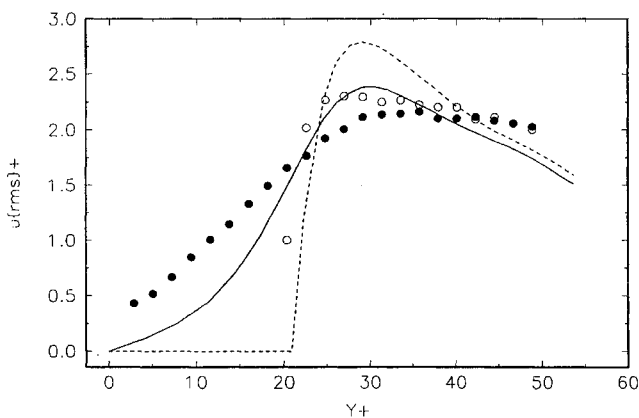


a) Nominal values  $s = 31$  and  $h = 21$

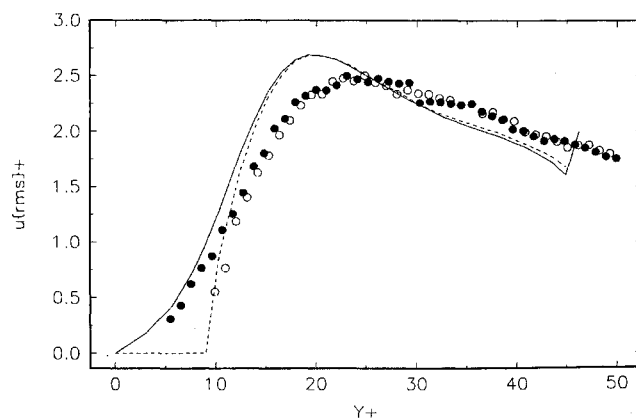


b) Nominal values  $s = 15$  and  $h = 9$

Fig. 5 Axial mean velocity distributions vs distance from the wall, relative to riblet peak ( $\circ$ , data and ---, calculations) and valley ( $\bullet$ , data and —, calculations).

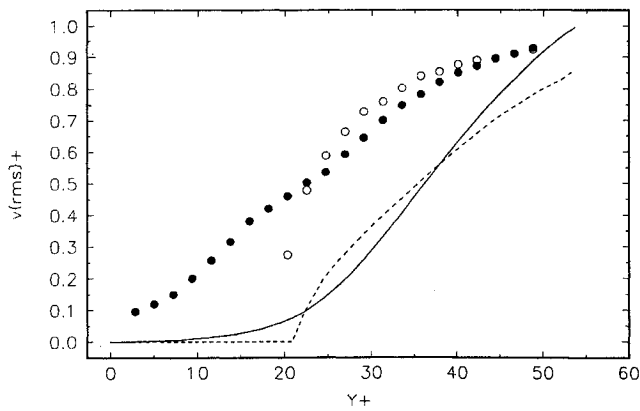
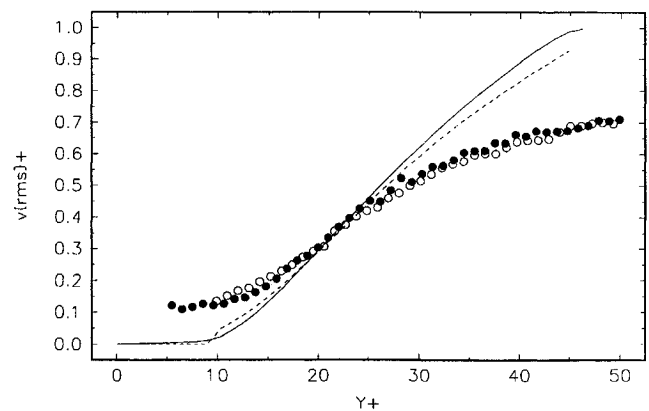


a) Nominal values  $s = 31$  and  $h = 21$

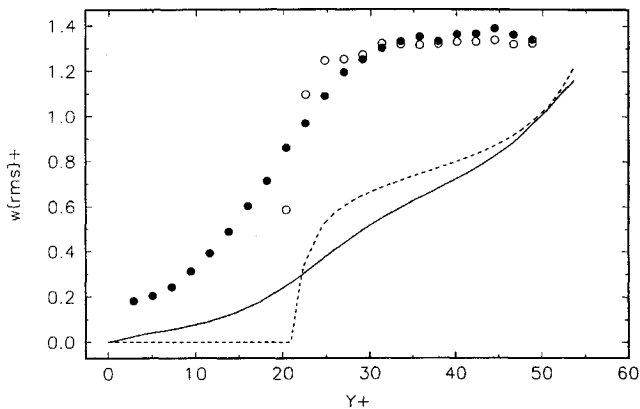
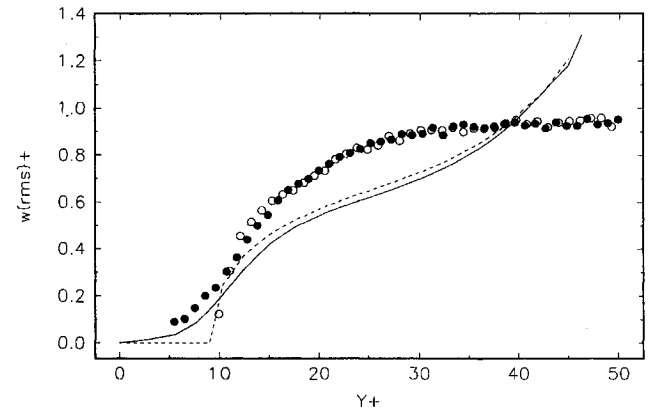


b) Nominal values  $s = 15$  and  $h = 9$

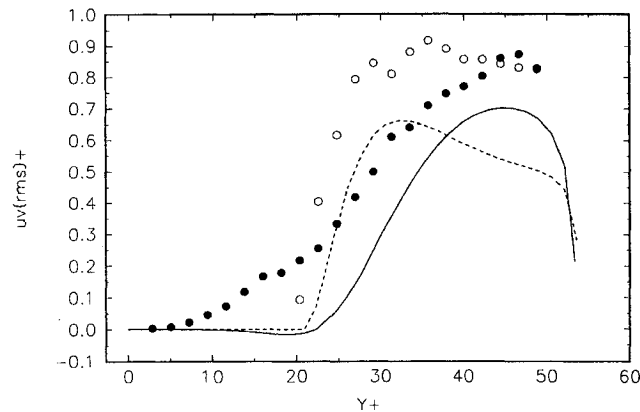
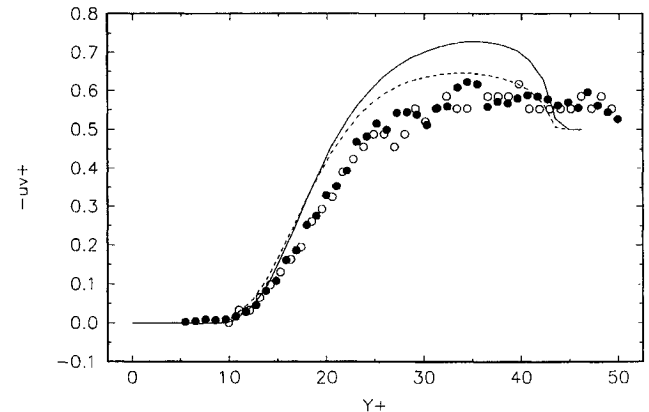
Fig. 6 Axial fluctuating velocity distributions vs distance from the wall, relative to riblet peak ( $\circ$ , data and ---, calculations) and valley ( $\bullet$ , data and —, calculations).

a) Nominal values  $s = 31$  and  $h = 21$ b) Nominal values  $s = 15$  and  $h = 9$ 

**Fig. 7** Transverse fluctuating velocity distributions vs distance from the wall, relative to riblet peak ( $\circ$ , data and ---, calculations) and valley ( $\bullet$ , data and —, calculations).

a) Nominal values  $s = 31$  and  $h = 21$ b) Nominal values  $s = 15$  and  $h = 9$ 

**Fig. 8** Spanwise fluctuating velocity distributions vs distance from the wall, relative to riblet peak ( $\circ$ , data and ---, calculations) and valley ( $\bullet$ , data and —, calculations).

a) Nominal values  $s = 31$  and  $h = 21$ b) Nominal values  $s = 15$  and  $h = 9$ 

**Fig. 9** Reynolds shear stress distributions vs distance from the wall, relative to riblet peak ( $\circ$ , data and ---, calculations) and valley ( $\bullet$ , data and —, calculations).

The wall normal or transverse and spanwise rms and the Reynolds shear stress are compared with the experimental data in Figs. 7–9. It is clear that the calculations and data compare poorly in magnitude but faithfully reflect the trends. That is, the wall normal velocity  $v_{rms}$ , the crossover between the velocity curves, occurs at the same  $y$  and follows reasonable well the wall normal evolution of the data. The  $w_{rms}$  also has the same trend as that for  $v_{rms}$ , except for  $y \geq 35$ , which is likely an effect of the periodicity in the large-scale outer flow imposed in the calculations. The Reynolds shear stress displays a remarkable similarity in wall normal evolution, showing as well that the stress is significantly greater over the riblet peaks. The data display some peculiar features, especially the spanwise velocity, which does not approach zero in the valleys, thereby perhaps confirming that the data are not statistically smooth, at least for the

larger riblets. Although not shown, the smaller riblet computations compare much better with the data, except, again, for the spanwise velocity, which displays similar trends to that already presented.

The results to be presented are plotted against distance normal to surface, in wall coordinates. The main points that this paper addresses can be succinctly made by considering thin element riblets of zero thickness, the compound thin element riblets with finite thickness, and a sample of those calculations that use flat valley V-groove riblets. The results to be presented arise from entries 3, 4, and 6 in Table 1.

Attention is focused first on comparing the calculations from the thin element (because of space limitations, these are not shown) and trapezoidal valley, Fig. 10 riblets, both with identical  $h^+$  and  $s^+$ . The main difference between the computational results is the

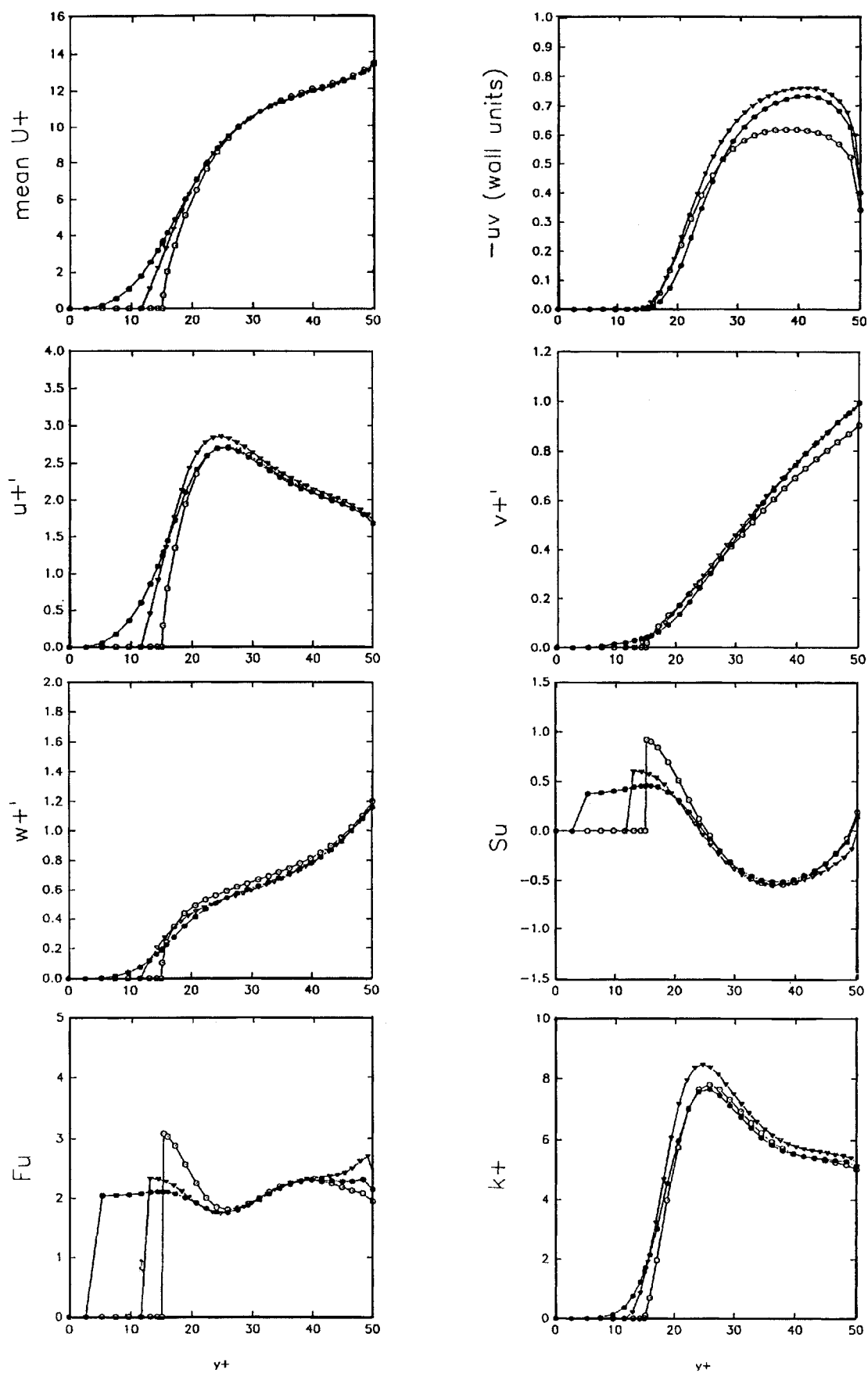


Fig. 10 Flat valley V-groove riblets: distributions of various variables vs distance from the wall, relative to riblet peak ( $\circ$ ) and valley ( $\bullet$ ) and flat wall ( $\nabla$ ):  $s = 20$ ,  $h = 15$ , and  $t = 0$ .

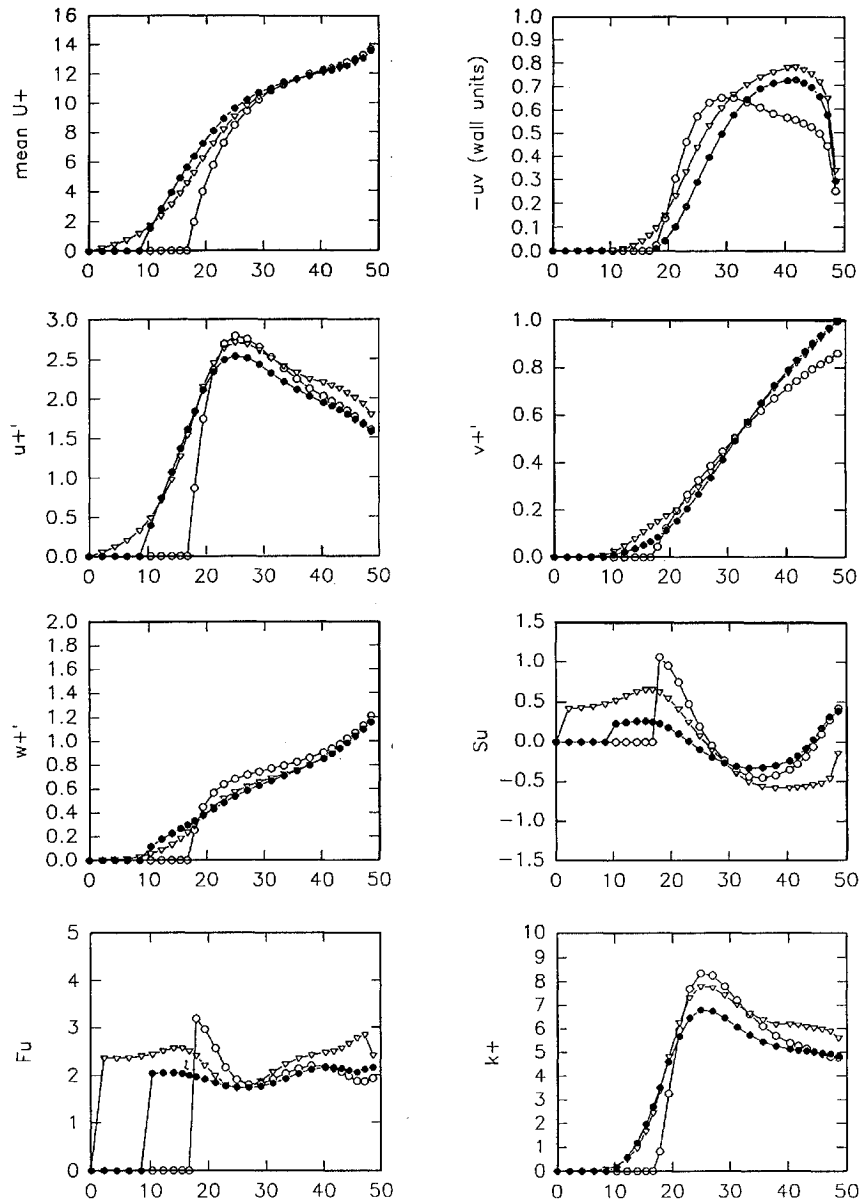


Fig. 11 Compound thin element riblets: distributions of various variables vs distance from the wall, relative to large riblet peak ( $\circ$ ) and valley ( $\nabla$ ) and above small riblet peak ( $\bullet$ ):  $s_1 = 33.3$ ,  $s_2 = 16.7$ ,  $h_1 = 16.7$ ,  $h_2 = 8.3$ , and  $t = 2.4$ . See Table 1.

trapezoidal valley riblets produce less kinetic energy and the location of the peak  $k^+$  is shifted farther away from the wall with concomitant drop in  $uv^+$ . More important still is that the skewness  $S_u$  is slightly larger over the peaks and slightly lower in the valleys than in the case of the thin element riblets. Although it is recognized that the method employed does not capture faithfully the skewness distribution in flat wall conditions (see Fig. 3), the trend is certainly well enough captured to permit a tentative extraction from the results that the trapezoidal valley riblets permit the outer, large-scale fluid to enter more readily the valley regions. So, although this may locally produce greater shear (at the tips), it is speculated that the most important feature is to ensure that the larger-scale outer eddies are kept away from the slower moving, low-momentum fluid inside the riblet valleys, thereby minimizing momentum exchange.

To test this argument, calculations are presented for the flow over compound element riblets, Fig. 11. These riblets are a development of those used by Wilkinson et al.<sup>40</sup> It is seen that  $uv^+$  distribution is altered favorably, the turbulence kinetic energy is reduced, and the skewness  $S_u$  is markedly reduced over a larger  $s^+$  than in the other examples.

The calculations reveal that riblets need not be uniform in height in the spanwise direction. The Reynolds shear stress in the riblet valleys is clearly reduced, but the near-wall viscous model cannot

provide much insight into the distributions of the wall normal or spanwise velocity skewness and flatness. Nor can it provide conclusive evidence that smaller-scale structural features participate in the near-wall skin-friction cycle. It can, however, ably demonstrate that secondary flows are generated within the riblet valleys by the QSWV but are short lived; however, during their lifetime they scoop out the low streamwise momentum fluid and create large shear around the tips of the riblets. It appears that an intermediate shorter riblet is sufficient to ensure that the low-momentum fluid within the valley remains mostly undisturbed and to force large spanwise scale motions away from the wall. Such multiple height riblets thus achieve the benefits of V- or U-groove profile forms.

The preceding sidesteps the issue of the effects of finite riblet thickness. In the calculations obtained to date, the riblet thickness seems to have little effect, provided this is in the limit of  $0 \leq t^+ \leq 2.4$ . This is encouraging for it is difficult to contemplate riblets for practical applications with  $t \rightarrow 0$ , which would be easily damaged. Thus, it is important for the future to examine double height V-groove forms.

## V. Conclusion

The paper has presented the results from applying a near-wall viscous region model to simulate the flow over riblets of various

cross-sectional shapes. The model has been demonstrated to faithfully reproduce the time-averaged characteristics obtained from a turbulent boundary layer. It has been applied successfully to a wall populated with riblets, assuming that the presence of riblets does not adversely affect the imposed boundary conditions at a height deduced using the protrusion height concept.

It has been demonstrated that, as the riblet spacing increases, the outer region QSWV can intrude into the valleys of the riblets and wash or scoop out the otherwise low-momentum fluid found there. The introduction of a smaller riblet, which replaces a normal height riblet, forces the QSWV to remain removed from the wall, thereby permitting a more continuous retention of low-momentum fluid. Although the skin friction over the peaks and in the valleys is larger and smaller, respectively, than that on a flat wall, it is the isolation of the wall from these incursions that plays a significant role in damping the near-wall turbulence activity.

### Acknowledgments

The financial support of NATO through a Collaborative Research and Development grant to the first and second authors is gratefully acknowledged. The financial support of the Natural Science and Engineering Research Council of Canada and Rolls Royce plc is also acknowledged. The authors are grateful to N. Kasagi and Y. Suzuki, University of Tokyo, for releasing their PTV data before publication as well as cultivating an atmosphere conducive for open collaboration. Part of this paper was written while the first author was on sabbatical at Centre D'Etudes Aerodynamique et Thermique, Université de Poitiers, France, and he acknowledges with sincere gratitude the fruitful and stimulating environment provided by all its members, in particular Jean Paul Bonnet and Joel Delville.

### References

- Coustols, E., and Savill, A. M., "Turbulent Skin-Friction Drag Reduction by Active and Passive Means," *Special Course on Skin Friction Drag Reduction*, edited by J. Coustix, Rept. 786. AGARD, March 1992.
- Walsh, M. J., "Riblets," *Viscous Drag Reduction in Boundary Layers*, edited by D. M. Bushnell and J. Hefner, Vol. 123, Progress in Astronautics and Aeronautics, AIAA, Washington, DC, 1990.
- Enyutin, G. V., Lashkov, Y. A., Samoilova, N. V., Fedeev, I. V., and Shumilkina, E. A., "Experimental Investigation of Turbulent Friction on Surfaces with Non-Continuous Riblets," *Scientific Letters of the CAGI*, Vol. 12, No. 3, 1991, pp. 43–50 (in Russian).
- Bechert, D. W., "Experiments on Three Dimensional Riblets," *Turbulent Drag Reduction by Passive Means*, Royal Aeronautical Society, London, 1987.
- Tullis, S., and Pollard, A., "Modeling the Time Dependent Flow over Riblets in the Viscous Wall Region," *Applied Scientific Research*, Vol. 50, 1993, pp. 299–314.
- Tullis, S., and Pollard, A., "A Numerical Investigation of the Turbulent Flow over V and U Groove Riblets Using a Viscous Wall Region Model," *Near Wall Turbulent Flows*, edited by R. M. C. So, C. G. Speziale, and B. E. Launder, Elsevier, Amsterdam, 1993, pp. 761–770.
- Tullis, S., and Pollard, A., "The Time Dependent Flow over V and U Groove Riblets of Different Sizes," *Physics of Fluids A*, Vol. 6, No. 2, 1994, pp. 1000, 1001.
- Chu, D. C., and Karniadakis, G. E., "A Direct Numerical Simulation of Laminar and Turbulent Flow over Riblet Mounted Surfaces," *Journal of Fluid Mechanics*, Vol. 250, 1993, pp. 1–42.
- Chu, D. C., Henderson, R., and Karniadakis, G. E., "Parallel Spectral Element Fourier Simulation of Turbulent Flow over Riblet Mounted Surfaces," *Theoretical and Computational Fluid Dynamics*, Vol. 3, 1992, pp. 219–229.
- Choi, H., Moin, P., and Kim, J., "Direct Numerical Simulation of Turbulent Flow over Riblets," *Journal of Fluid Mechanics*, Vol. 255, 1993, pp. 503–540.
- Tang, Y. P., and Clark, D. G., "On Near Wall Turbulence-Generating Events in a Turbulent Boundary Layer on a Riblet Surface," *Applied Scientific Research*, Vol. 50, 1993, pp. 215–232.
- Suzuki, Y., and Kasagi, N., "Drag Reduction Mechanism on Micro-Grooved Riblet Surface," *Near Wall Turbulent Flows*, edited by R. M. C. So, C. G. Speziale, and B. E. Launder, Elsevier, Amsterdam, 1993, pp. 709–718.
- Choi, K. S., "Near-Wall Structure of a Turbulent Boundary Layer with Riblets," *Journal of Fluid Mechanics*, Vol. 208, 1989, pp. 417–458.
- Tardu, S., Truong, T. V., and Tanguay, B., "Bursting and Structure of the Turbulence in an Internal Flow Manipulated by Riblets," *Applied Scientific Research*, Vol. 50, 1993, pp. 189–213.
- Benhalilou, M., Anselmet, F., Liandrat, J., and Fulachier, L., "Experimental and Numerical Investigation of a Turbulent Boundary Layer over Riblets," *Proceedings of the 8th Symposium on Turbulent Shear Flows* (Munich, Germany), Technical Univ. of Munich, Germany, 1991, pp. 18-5-1–18-5-6 (Paper 18).
- Pulles, C. J. A., Krishna Prasad, K., and Nieuwstadt, F. T. M., "Turbulence Measurements over Longitudinal Micro-Grooved Surfaces," *Applied Scientific Research*, Vol. 46, 1989, pp. 197–208.
- Falco, R. E., "A Coherent Structure Model of the Turbulent Boundary Layer and Its Ability to Predict Reynolds Number Dependence," *Philosophical Transactions of the Royal Society London, Series A: Mathematical and Physical Sciences*, Vol. 336, 1991, pp. 103–129.
- Smith, C. R., Walker, J. D. A., Haidari, A. H., and Sobrun, U., "On the Dynamics of Near Wall Turbulence," *Philosophical Transactions of the Royal Society London, Series A: Mathematical and Physical Sciences*, Vol. 336, 1991, pp. 131–175.
- Morrison, J. F., Subramanian, C. S., and Bradshaw, P., "Bursts and the Law of the Wall in Turbulent Boundary Layers," *Journal of Fluid Mechanics*, Vol. 241, 1992, pp. 75–108.
- Luchini, P., Manzo, F., and Pozzi, A., "Resistance of a Grooved Parallel Flow and Cross-Flow," *Journal of Fluid Mechanics*, Vol. 228, 1991, pp. 87–109.
- Smith, C. R., and Metzler, S. P., "The Characteristics of Low-Speed Streaks in the Near-Wall Region of a Turbulent Boundary Layer," *Journal of Fluid Mechanics*, Vol. 129, 1983, pp. 27–54.
- Kasagi, N., "Structural Study of Near-Wall Turbulence and Its Heat Transfer Mechanism," *Near Wall Turbulence, 1988 Zoran Zaric Memorial Conference*, edited by S. J. Kline and N. Afgan, Hemisphere, New York, 1990.
- Robinson, S. K., "The Kinematics of Turbulent Boundary Layer Structure," NASA, TR TM-103859, April 1991.
- Bechert, D. W., and Bartenwerfer, M., "The Viscous Flow on Surfaces with Longitudinal Ribs," *Journal of Fluid Mechanics*, Vol. 206, 1989, pp. 105–129.
- Bruse, M., Bechert, D. W., van der Hoeven, J. G., Hage, W., and Hoppe, G., "Experiments with Conventional and with Novel Adjustable Drag-Reducing Surfaces," *Near Wall Turbulent Flows*, edited by R. M. C. So, C. G. Speziale, and B. E. Launder, Elsevier, Amsterdam, 1993, pp. 719–738.
- Wilkinson, S. P., and Lazos, B. S., "Direct Drag and Hot Wire Measurements on Thin Element Riblet Arrays," *IUTAM Symposium on Turbulence Management and Relaminarisation*, edited by H. Liepmann and R. Narasimha, Springer-Verlag, Heidelberg, Germany, 1987, pp. 121–132.
- Savill, A. M., "Control of Fluid Flow," U.S. Patent No. TR 4,930,729, June 1990.
- Chapman, D. R., and Kuhn, G. D., "The Limiting Behavior of Turbulence Near a Wall," *Journal of Fluid Mechanics*, Vol. 170, 1986, pp. 265–292.
- Nikolaides, C., "A Study of the Coherent Structures in the Viscous Wall Region of a Turbulent Flow," Ph.D. Dissertation, Dept. of Chemical Engineering, Univ. of Illinois, Urbana, IL, 1984.
- Tullis, S., "Modelling the Time Dependent Flow over Riblets in the Viscous Wall Region," M.S. Thesis, Dept. of Mechanical Engineering, Queen's Univ. at Kingston, ON, Canada, 1992.
- Saabas, H. J., "A Control Volume Based Finite Element Method for Three-Dimensional, Incompressible, Viscous Fluid Flow," Ph.D. Dissertation, Dept. of Mechanical Engineering, McGill Univ., Montreal, PQ, Canada, 1991.
- Gupta, A. K., and Kaplan, R. E., "Statistical Characteristics of Reynolds Stress in a Turbulent Boundary Layer," *Physics of Fluids*, Vol. 15, No. 15, 1972, pp. 981–985.
- Ueda, H., and Hinze, J. O., "Fine-Structure Turbulence in the Wall Region of a Turbulent Boundary Layer," *Journal of Fluid Mechanics*, Vol. 67, 1975, pp. 125–143.
- Baron, A., and Quadrio, M., "Some Preliminary Results on the Influence of Riblets on the Structure of a Turbulent Boundary Layer," *International Journal of Heat and Fluid Flow*, Vol. 14, No. 3, 1993, pp. 223–230.
- Willmarth, W. W., and Tu, B. J., "Structure of Turbulence in the Boundary Layer near the Wall," *Physics of Fluids*, Vol. 10, 1967, pp. S134–S141.
- Vukoslavčević, P., Wallace, J. M., and Balint, J.-L., "On the Mechanism of Viscous Drag Reduction Using Streamwise Aligned Riblets: A Review with New Results," *Turbulent Drag Reduction by Passive Means*, Royal Aeronautical Society, London, 1987, pp. 290–309.
- Tang, Y. P., and Clark, D. G., "On Turbulence Generating Events over Drag Reducing Riblets," Queen Mary and Westfield College, Univ. of London, TR QMW-EP-1087, 1991.
- Suzuki, Y., and Kasagi, N., "On the Drag Reduction Mechanism Above a Riblet Surface," AIAA Paper 93-3257, 1993.
- Park, S.-R., and Wallace, J. M., "Flow Alteration and Drag Reduction by Riblets in a Turbulent Boundary Layer," *AIAA Journal*, Vol. 32, No. 1, 1994, pp. 31–38.
- Wilkinson, S. P., Anders, J. B., Lazos, B. S., and Bushnell, D. M., "Turbulent Drag Reduction Research at NASA Langley—Progress and Plans," *International Journal of Heat and Fluid Flow*, Vol. 9, 1989, pp. 266–277.